Materials and Design 186 (2020) 108317

Contents lists available at ScienceDirect

Materials and Design

journal homepage: www.elsevier.com/locate/matdes

In-process spectroscopic detection of chromium loss during Directed Energy Deposition of alloy 718

Agnieszka Kisielewicz [a,*], Esmaeil Sadeghi [a], Fredrik Sikström [a], Anna-Karin Christiansson [a], Gianfranco Palumbo [b,c], Antonio Ancona [a,c]

[a] University West, Department of Engineering Science, Gustava Melins Gata 2, 461-32, Trollhättan, Sweden
[b] DMMM, Politecnico di Bari, Viale Japigia 182, 70126, Bari, Italy
[c] CNR-IFN Institute for Photonics and Nanotechnologies, Physics Department, Via Amendala 173, 70126, Bari, Italy

HIGHLIGHTS

- An in-process monitoring system based on a spectrometer allows detecting variation in processing conditions during DED.
- Spectroscopic data indicates viporazation and depletion of vital alloying elements from the deposited material.
- The system has a high sensitivity, as conditions leading to changes of less than 1 wt% of chromium content were detected.

GRAPHICAL ABSTRACT

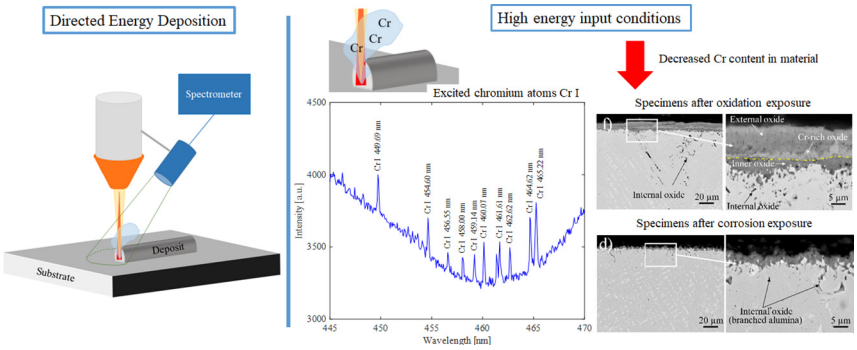

ARTICLE INFO

Article history:
Received 15 July 2019
Received in revised form 9 October 2019
Accepted 28 October 2019
Available online 09 November 2019

Keywords:
spectroscopic system
Additive manufacturing
Directed energy deposition
Cr depletion
High-temperature corrosion

ABSTRACT

In this work, a fast optical spectrometer was used to monitor the Directed Energy Deposition (DED) process, during the deposition of Alloy 718 samples with different laser power, thus different energy inputs into the material. Spectroscopic measurements revealed the presence of excited Cr I atoms in the plasma plume. The presence was more apparent for the samples characterized by higher energy input. The Cr depletion from these samples was confirmed by lower Cr content detected by Energy-Dispersive X-ray Spectroscopy (EDS) analysis. The samples were also characterized by higher oxidation and high-temperature corrosion rates in comparison to the samples produced with low energy input. These results prove the applicability of an optical emission spectroscopic system for monitoring DED to identify process conditions leading to compositional changes and variation in the quality of the built material.

1. Introduction

Aerospace applications impose strict requirements on the materials applied for the load-bearing aircraft components due to the harsh operating conditions. Turbojet engines, specifically, are examples of such challenging applications where the components must withstand high loads at the elevated operating temperatures close to the melting point of the materials. What is more, the parts often experience inelastic and irreversible deformation over long time periods (creep), when a strain accumulation occurs [1]. The environmental factors, including moisture, high temperature and a presence of corrosive agents,

* Corresponding author.
E-mail address: agnieszka.kisielewicz@hv.se (A. Kisielewicz).

https://doi.org/10.1016/j.matdes.2019.108317

contained in both engine fuel and intake air, create favorable conditions for accelerated oxidation and high-temperature corrosion. Therefore, for manufacturing elements of turbojet engines, like final stages of a compressor, combustors and turbine sections, nickel-and nickel-iron based superalloys are used due to their ability to maintain enough creep resistance as well as to protect against corrosion at elevated temperatures.

Alloy 718 is a nickel-iron superalloy characterized by high toughness and ductility as well as good weldability [2]. The main alloying elements of the alloy are nickel (Ni), iron (Fe) and chromium (Cr). Ni is the element that has the highest content in the alloy and is the component of the main phases like γ, γ' and γ". Fe content helps to improve workability as well as to decrease the cost of the material. The considerably high content of Cr (17–21 wt%) improves high-temperature corrosion performance of materials, including hot corrosion and oxidation behaviors [2].

Until very recently, most of the vital parts of turbojet engines were produced from wrought materials [2] since the conventional manufacturing methods, e.g. forging and rolling, provide good control over material composition, grain size as well as the overall material morphology. However, the recent 20-years development of Additive Manufacturing (AM) technologies encourages aircraft engine manufacturers to replace parts and components produced by the conventional methods with those produced by additive technologies. This change is driven by the broader manufacturing possibilities of AM technologies, such as the production of more complex shapes, the reduction of the number of parts, the flexibility of the methods as well as the cost-efficiency related to the reduction of the overall production cost and the buy-to-fly ratio [3]. Despite the fact that metal AM installations around the world have witnessed impressive growth in the past few years and the field has been the subject of significant research efforts, a number of generic technology-related hurdles remain yet to be overcome before it can make a significant impact for the manufacturing industry. A common challenge is to gain a better understanding of the relationship between the process parameters, microstructure and properties of the AM materials. It has been understood that many of the physical processes occurring during AM are nearly identical to those characteristics of welding technologies. Thereby, the influence of process parameters on microstructure, material properties, defect formation and melt pool behavior are expected to be similar for both technologies [4].

One of the phenomena present in both welding and AM is vaporization of major alloying elements from the material during processing. The vaporization occurs when a high-density energy source, like a laser beam, melts the material, heating it to temperatures above the melting point of its alloying elements. As a consequence, the material undergoes a compositional change that can highly affect its final properties. This phenomenon was already investigated for welding, e.g. in the work [5], it was reported that the rate of vaporization during laser beam welding (LBW) of stainless steel depends on the applied laser power. Increased laser power induces higher vaporization related to the increase in the temperature of the weld pool.

During the Directed Energy Deposition (DED) using laser beam and powder, crucial elements contained in the processed alloy can vaporize not only from the melt pool [4], but also directly from the powder particles, while they travel through the laser beam [6]. Recognizing the high impact of the vaporization phenomenon on properties of the AM materials, the susceptibility of several alloys to the loss of alloying elements was studied [7]. The investigation of three different types of alloys: stainless steel, titanium-based and nickel-based alloys, revealed that the latter has the lowest susceptibility to vaporization. Nevertheless, the calculation of the rate of vaporization of selected alloying elements and experimental data indicated a loss of Cr from the nickel-based alloy. Since, among the three most dominant alloying elements: Ni, Fe and Cr, the latter has the highest equilibrium vapor pressure at elevated temperatures, it is the most prone to vaporization.

As aforementioned, Cr plays a vital role in the corrosion behavior of superalloys. As alloying element, it assists formation of a dense and continuous chromia (Cr_2O_3) scale that protects the material against the corrosion attack [2]. Studies on nickel-based and cobalt-based superalloys show that the materials characterized by a Cr content above 15 wt% are much less sensitive to corrosion compared to the ones with the lower Cr content [8]. The most common type of corrosion in turbojet engines is the high-temperature corrosion, so-called "hot corrosion" [8]. Depending on the different temperatures ranges and the mechanism of material degradation, one can distinguish two sorts of hot corrosion, Type I and Type II. Type I hot corrosion typically occurs in turbojet engines at the temperature range between 800 °C and 950 °C, though the range can vary depending on the alloy in focus.

Considering the vaporization of alloying elements during fabrication with AM processes and its consequences in terms of compositional changes of the built part, it is of great relevance to develop an in-process monitoring system that could allow detection of the loss of alloying elements already during deposition. Since the plasma formed above the melt pool is strongly related to the vaporization phenomenon, an appropriate strategy of process monitoring would include the detection of the plasma optical emission. The plasma emission analysis has already been performed for both welding and AM by means of optical spectroscopy. In the work [9], a spectrometer was used to analyze the radiation emitted by the weakly ionized plasma created during LBW in a wide spectral range from 200 to 1100 nm. The researchers reported presence of spectral lines indicating excited and ionized species in the plasma, however no further analysis of the spectral lines was described. Similar findings were reported for DED process [10]. The analysis of the acquired spectra in the visible range of the electromagnetic radiation allowed to recognize distinct spectral lines associated to excited Cr atoms. The author suggested that the spectral lines could be an indication of a compositional change in the built material. However, no further investigation was reported. On the other hand, based on detected spectral lines of excited Cr and Fe atoms, a real-time Cr composition's prediction system for alloys with well-known material composition was developed [11]. The system was validated on pure Cr and tool steel alloy samples. Nonetheless, no influence of process parameters on the accuracy of the system was presented. The radiation from the melt pool acquired during DED process was also spectrally analyzed to estimate its temperature [12]. In other work [13], the authors used spectral lines identified during DED depositions to establish a relationship between spectral parameters, like line intensity ratio and electron temperature, and geometrical features, e.g. the aspect ratio of the built samples. They concluded that using the spectral information can help to monitor not only the melt depth but also the onset of the metallic bonding between the substrate and the powder material. Their analysis of the built material was restricted to the geometry of the deposited beads. A different approach was presented in Ref. [14], where the authors analyzed the plasma created during the deposition process of titanium-based alloy in order to find indications of defects, like e.g. lack-of-fusion, during the building. The analysis of spectroscopic data and images from a CCD camera indicated variations in the plasma plume as the process parameters were changed as well as when a defect occurred in the material.

Despite the fact that optical spectroscopy has already been applied for monitoring of laser-based AM processes [10,12,13], some information was found correlating the spectroscopic data to critical properties of the built material, like e.g. microstructure and hardness [15], however not to corrosion behavior.

This paper presents an experimental investigation of the relationship between the presence of characteristic atomic Cr emission spectral lines, indicating the presence of the element in the weakly ionized plasma plume created during DED of Alloy 718, and the depletion of this element from the built due to vaporization. For this purpose, DED experiments were performed by varying the laser power and thus the energy input delivered into the material. In addition, it was investigated

how the change of the Cr content of the deposited material affects its oxidation and corrosion resistance at high temperatures.

2. Experimental setup and procedures

This section contains a detailed description of the experimental setup established for DED experiments with the in-process spectroscopic system as well as sample preparation and material characterization procedures.

2.1. Laser and spectroscopic monitoring systems

The experimental setup consisted of a CNC machine, a 6 kW fiber laser, a coaxial annular powder nozzle with a powder feeder and a monitoring system based on a high-resolution spectrometer.

The CNC gantry machine from Isel® Germany (mod. M40) was used to maneuver the coaxial powder nozzle and the laser optics that were mounted on the tool holder attached to the Z-axis of the machine. The laser beam, generated by the continuous wave 6 kW IPG Ytterbium-doped Fiber Laser (mod. YLR-6000-S) with a 1070 nm wavelength, was guided through an 800 μm core optical fiber to the optics connected to the powder nozzle. The focused beam was characterized by a Rayleigh length equal to 3.73 mm and a spot size diameter in the focal plane equal to 0.75 mm. The values characterizing the laser beam were experimentally obtained during beam characterization performed using PRIMES (mod. FocusMonitor FM35). The laser focal point was positioned at the tip of the nozzle. The nozzle was a commercially available tool produced by Fraunhofer ILT (mod. COAX-40), allowing focusing the blown powder into a fine spot with the diameter smaller than 1 mm. Considering the possibility of overheating the tool during the deposition process, the nozzle was water-cooled during the entire process. The Uniquecoat volumetric powder feeder (mod. PF50WL) was used to supply the powder to the nozzle. The depositions were performed in inert, argon gas atmosphere. The additional function of the gas was to transport powder particles into the laser-matter interaction zone. The material of both the powder and the substrates used in the experiments was Alloy 718. The powder was characterized by the apparent density of 4.73 g/cm^3 and the particle distribution between 38 μm and 125 μm.

The core of the monitoring system was a commercially available Ocean Optics spectrometer (mod. HR2000+) equipped with a 2048 pixel CCD array detector and a 10 μm entrance slit. The sensor operated in the visible range of the electromagnetic spectrum between 400 nm and 530 nm, with a spectral resolution of 0.07 nm. During the experiments, the exposure times were optimized in order to exploit the full dynamic range of the spectrometer in each process condition. Thus, a short exposure time of 20 ms was selected during the deposition with high energy input (see Table 1), to avoid saturation of the signals, whereas the exposure time was increased to 300 ms for the experiments with the low energy input (see Table 1), which enabled capturing enough light. A 6-mm-focal-length collimator connected to a 100-μm-core optical fiber was used to collect light and send it to the spectrometer. The collimator was attached to the deposition nozzle and placed off-axis, at a polar angle of 30° to the laser beam and azimuthal angle of 15° to the deposition path. This configuration allowed the collection of radiation emitted from the laser-matter interaction zone, melt pool as well as the plasma plume above it. A protective glass was mounted on the collimator to shield it from potential spatters created during the deposition process. The spectrometer was connected to a PC via a USB connection. The signals were displayed and saved during the deposition process by a dedicated application developed in a LabVIEW environment. The schematic view of the setup is presented in Fig. 1.

The analysis of the spectra acquired during the deposition was performed offline. The identifications of the spectral lines were based on information contained in the National Institute of Standards and Technology (NIST) Atomic Spectra Database [16] as well as the chemical composition of the material and physical characteristics of the alloying elements. In particular, the equilibrium vapor pressures [7] of the three most dominant alloying elements of the Alloy 718 at elevated temperatures were taken into account during the spectral lines' identification.

2.2. DED experimental procedure

The laser process parameters were defined based on results from the Design of Experiments analysis reported in the work of Segerstark et al. [17] performed in similar experimental conditions. Specifically, two sets of process parameters, settings 1 and settings 2 (see Table 1), characterized by the low and the high energy inputs, respectively, were selected with to compare the response of the in-process spectroscopic monitoring system during two significantly diverse process conditions.

For each process setting, multiple layers and beads were deposited on a substrate (size: 300 mm × 40 mm × 3 mm) to create rectangular samples characterized by approximate dimensions of 35 mm × 7 mm × 5 mm. Taking into account the fact that a change of laser power, with all other parameters maintained constant, has a considerable influence on the shape of the beads, two different depositions patterns needed to be applied. In particular, for settings 1 (the low energy input), 17 layers with 6 beads in each layer were deposited while for settings 2 (the high energy input) the number of deposited layers was 25 with 3 beads in each layer.

2.3. Material characterization

The as-built samples were sectioned by water jet cutting (WJC) and afterward segmented using a diamond-tipped precision saw to extract several specimens for further analyses and characterizations described below.

One part of the specimens of material in as-built conditions was analyzed using an X-ray diffractometer (XRD) produced by Siemens (mod. D5000), equipped for grazing incidence analysis with Cu-Kα radiation of wavelength $\lambda = 0.154$ nm operating with a fixed incident angle of 1° and diffraction angle (2θ) between 25° and 80°. The step size and counting time per step were 0.02 (°) and 2 s, respectively. The analysis of the diffractograms was performed with DIFFRAC.EVA software using the ICDD-PDF database for phase identification. The phases of crystalline materials were identified by comparing a collected diffraction pattern with a reference pattern of a known material in the database. Additionally, another part of the specimens in as-built conditions was mounted and grinded/polished with a 0.2 μm colloidal silica finish before being analyzed using a Zeiss Optical Microscope (mod. EVO 50) and a Field Emission Scanning Electron Microscope from Zeiss (mod. Sigma) and an Energy-Dispersive X-ray Spectroscopy module (mod.

Table 1
Selected process parameters representing the low energy input (settings 1) and the high energy input (settings 2) conditions.

	Laser power [W]	Scanning speed [mm/s]	Powder feed rate [g/min]	Powder focal distance[a][mm]	Laser standoff distance[b][mm]
Settings 1	500	17.5	6	0	7
Settings 2	1400	17.5	6	0	7

[a] Distance between the powder focal point and the material surface.
[b] Distance between the laser focal point and the material surface.

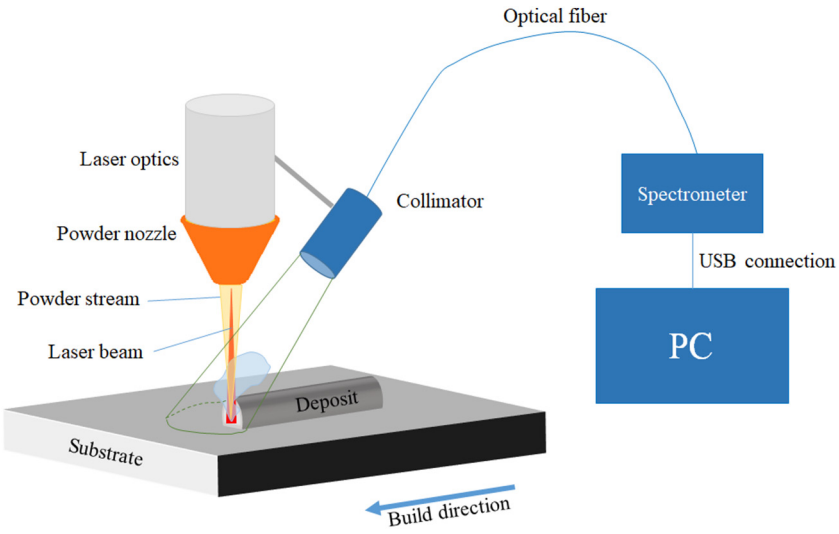

Fig. 1. Schematic diagram of the DED experimental setup, including the in-process monitoring system.

INCA X-Act) from Oxford Instruments for microstructural and compositional evaluation, respectively. For the SEM analyses, the backscattered electron (BSE) signals were used at an accelerating voltage of 15 kV in order to improve the spatial resolution, while the EDS measurements were performed using an accelerating voltage of 20 kV and the Aztec software from Oxford Instruments to acquire and process the spectra.

The remaining, unmounted specimens were subjected to isothermal oxidation and hot corrosion exposures in a box furnace. The specimens were placed in separate alumina crucibles and inserted into the furnace at a selected temperature. The oxidation tests were performed in static, ambient air at the temperatures of 700, 800, and 900 °C for 168 h. The hot corrosion tests were conducted in similar conditions with the addition of Na_2SO_4 salt at two temperature levels, 700 and 900 °C, addressing hot corrosion types I and II [8]. A Na_2SO_4 suspension was prepared with ethanol, and the solution (~0.1 mg/cm^2) was applied on all surfaces of the specimens using a paintbrush. Just before the test, each specimen and each crucible was individually weighed using a Sartorius™ balance (mod. Cubis MSA3.6P0TRDM) with microgram resolution. The crucible and specimen with the solution were also weighed together to calculate the exact amount of the solution placed on each specimen. The surface of the specimens was also measured before the exposure. After the test, the specimens were extracted from the furnace, weighed in their individual crucibles together with the oxide scale or corrosion products formed during the exposures. The weight change of the specimens per unit area, as well as the quality of oxide scale or corrosion product generated during the exposure, was used as the base for further evaluation.

The exposed specimens were then cut and cold mounted for further cross-sectional evaluation in a low shrinkage resin to prevent the spallation of the formed oxide scale. SEM as well as XRD analyses were performed on the exposed specimen cross-sections to compare the phases present after the high-temperature corrosion with the ones detected in the unexposed specimens. For the XRD measurements, a low incidence angle was selected in order to penetrate only the most outer layer of material composed of oxides and corrosion products.

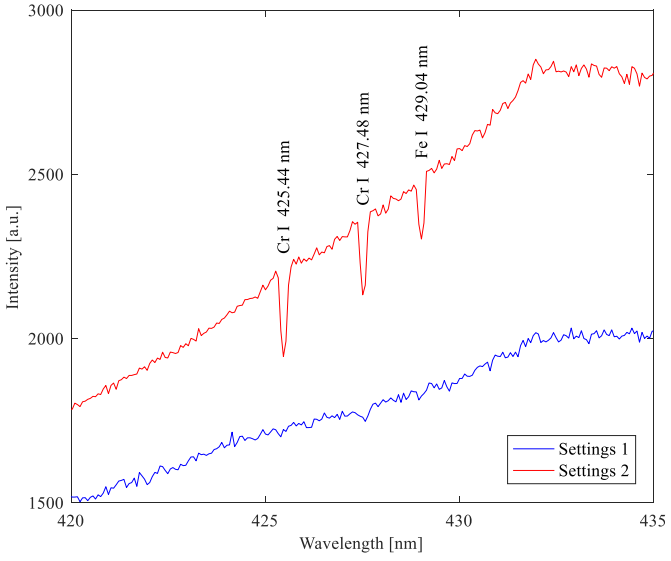

Fig. 2. Representative optical emission spectra acquired during deposition with the low energy input (settings 1) and the high energy input (settings 2) in the spectral region where the absorption lines were detected.

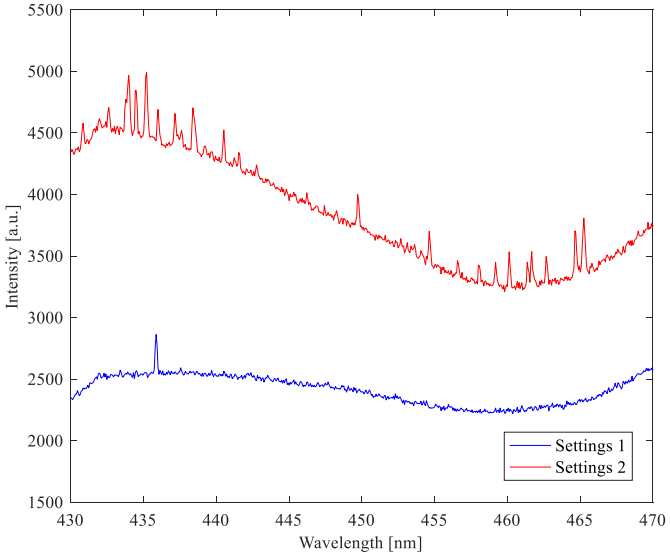

Fig. 3. Representative optical emission spectra acquired during deposition with the low energy input (settings 1) and the high energy input (settings 2) in the spectral region where most of the emission lines were detected.

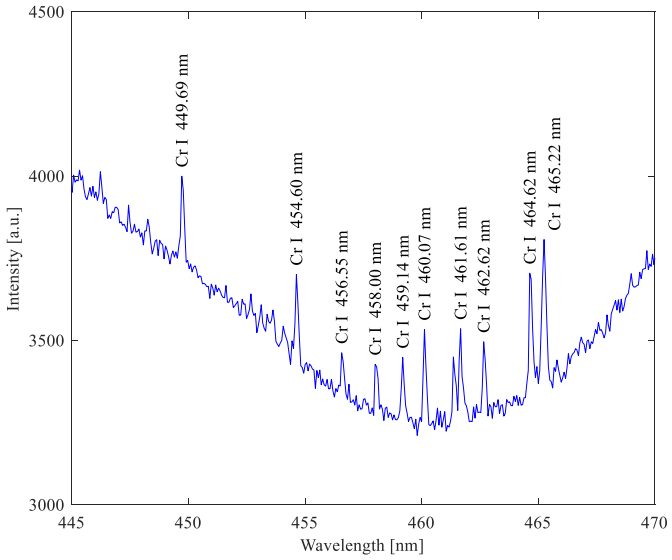

Fig. 4. Representative optical emission spectrum acquired during deposition with the high energy input (settings 2), showing the identified Cr emission lines.

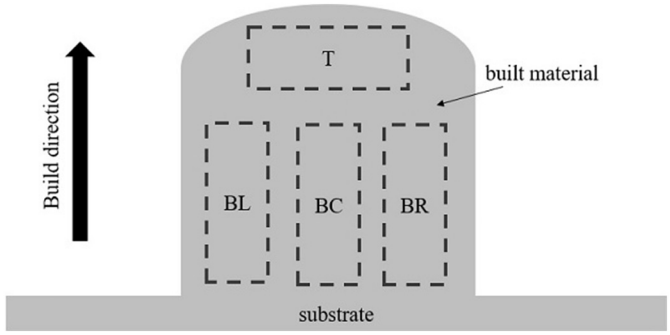

Fig. 6. Schematic view of a cross-section of a sample with marked by dashed lines areas selected for evaluation of chemical composition. The top, bottom-left, bottom-center and bottom-right areas are indicated by letters T, BL, BC and BR, respectively.

3. Results

3.1. Spectral emissions during deposition

The emission spectra collected during the deposition process were analyzed investigating the presence of distinctive absorption or emission spectral lines to gain information on the vaporized elements present in the plasma plume. Spectra acquired under the low energy input (settings 1) were compared with the ones with the high energy input (settings 2). Fig. 2 shows representative spectra in the wavelength range from 420 to 435 nm collected during depositions with the high and the low energy inputs. One can clearly distinguish absorption lines appearing as three consecutive dips in the continuum radiation related to the high energy input conditions. Absorption lines appear when vaporized atoms absorb photons radiated from the laser-matter interaction zone and become excited. Further identification analysis, based on NIST Atomic spectra database, revealed that the lines appearing at the wavelengths of 425.44 and 427.48 nm are related to excited Cr atoms (Cr I), while the line at 429.04 nm belongs to the excited Fe atom (Fe I). The presence of excited atoms indicates the existence of a laser-induced, weakly ionized plasma generated above the melt pool containing the alloying elements vaporized from the melting powder. All spectral signals acquired during the deposition with the high energy input were characterized by the presence of the absorption lines. No absorption or emission lines were observed in the same region of the electromagnetic spectra during the deposition of material with the low energy input.

Emission lines, related to de-excitation of vaporized atomic or ionic species in the plasma plume, were also observed in the spectra acquired during deposition with both process settings. However, while only two distinct emission lines (one of which ascribed to Cr I) were detected in case of the experiments with the low energy input (settings 1), considerably larger number of lines was observed for the experiments with the high energy input (settings 2), as shown in Fig. 3.

Specifically, twenty-one different spectral lines were revealed in the wavelength range between 425 nm and 470 nm. Sixteen of these were identified as Cr I. The most densely populated region of the spectra with identified Cr lines is presented in Fig. 4. The simultaneous detection of several absorption and emission lines during deposition with the high energy input indicates the presence of plasma over the melt pool. Since most of the lines belong to Cr I species, it can be concluded that such plasma is rich in vaporized Cr atoms, which is an indication of depletion of Cr element from the deposited material. For depositions with the low energy input, no absorption lines and very few emission lines were observed, which is why it can be assumed that in this case the rate of element vaporization is much lower.

3.2. Characterization of as-built material

In this section, the results of the characterizations of the materials deposited with the two different process settings are presented.

The optical microscope and SEM (BSE mode) analyses revealed several differences between material built with the high and the low energy input. Fig. 5 shows micrographs of the material obtained during the analyses with the optical microscope and SEM. The specimens built with the low energy input were characterized by regularly distributed heat-affected zones corresponding to the selected deposition pattern, see Fig. 5 a1. Whereas, in case of the high energy input specimens, the positioning of the heat-affected zones

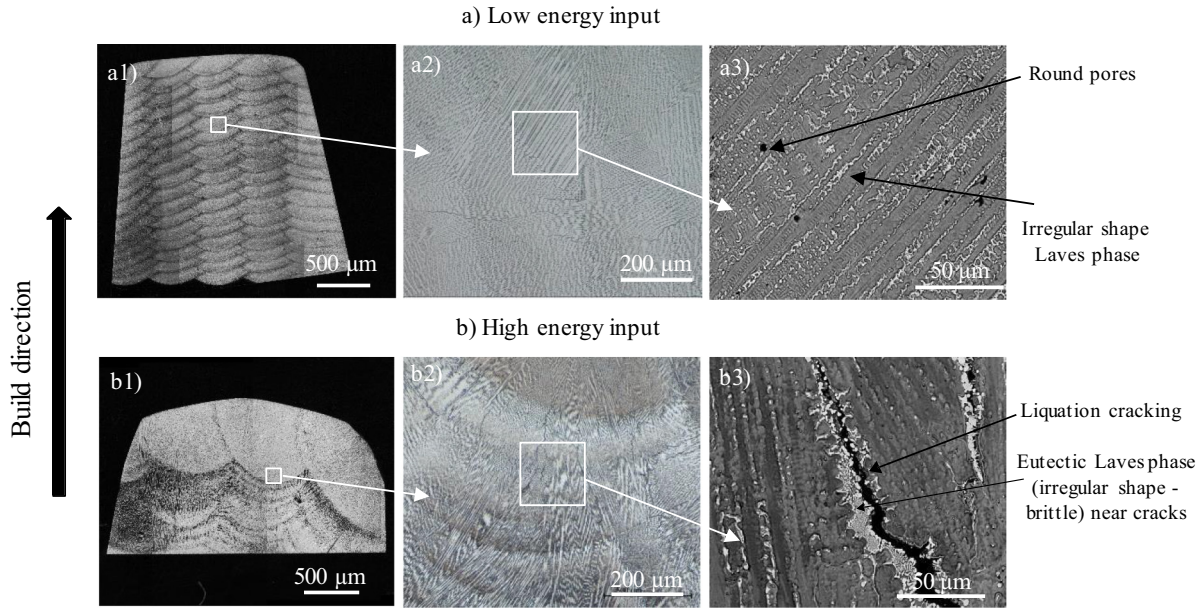

Fig. 5. Optical microscope and SEM micrographs of the cross-sections of (a) material built with process settings 1 (a1, a2, and a3), (b) material built with process settings 2 (b1, b2, and b3).

Table 2
Results of EDS analyses of the specimens in as-built conditions: average value in wt% (standard deviation).

	Ni	Cr	Fe	Nb	Rest of elements
Settings 1	50.33 (0.73)	19.59 (0.39)	18.57 (0.59)	5.12 (0.45)	6.40
Settings 2	49.87 (1.06)	19.05 (0.17)	18.43 (0.59)	5.19 (0.43)	7.47

and their irregular shape indicated instances of re-melting of several layers of material, see Fig. 5 b1. Despite the fact that in all specimens, internal flaws were found, the defects present in specimens produced with the high energy input were more determining. Thus, the presence of liquation cracking surrounded by the brittle Laves phase can highly impair fatigue properties of the material as, if being subjected to tensile loads, the crack is likely to propagate, see Fig. 5 b2-b3. Whereas round pores, present in samples produced with the low energy input, can be considered as non-determining flaws depending on the final application of the material, see Fig. 5 a2-a3.

For the EDS characterization, several cross-sections were analyzed. For each specimen, four different areas (with dimensions of around 1.5 mm × 2 mm), located respectively at the top, bottom-left, bottom-center and bottom-right of the metallographic cut (see Fig. 6), were selected and the average chemical composition was measured. No significant difference was found in the composition of the different selected areas. Therefore, in Table 2, values of the weight % of the main alloying elements such as Ni, Cr, Fe and niobium (Nb) averaged over several specimens and different areas are reported. It can be observed that the specimens extracted from samples built with the high energy input (settings 2) are characterized by lower Cr content, which is in line with the indications of the spectroscopic measurements.

Fig. 7 shows the XRD patterns of feedstock powder and as-built DED specimens built with the low and the high energy input. Three primary peaks of the powder (2θ (°) ≈ 43.5, 51.0, and 74.7) are attributed to the austenitic γ-Ni(Cr) phase. The powder presented a very low level of oxides, indicated by the Al2O3 peaks, which were not present for the specimens in as-built conditions. This was most probably due to the low vapor pressure of such oxides at DED processing conditions [18]. The as-built specimens retained the primary solid solution phase of the feedstock powder. No peak broadening was observed in the XRD patterns of the specimens, meaning no significant change occurred in the crystallite size of the specimens produced with different energy input. The XRD peaks verified that all the specimens had almost similar phase content and a similar level of residual stresses before the oxidation and hot corrosion exposures.

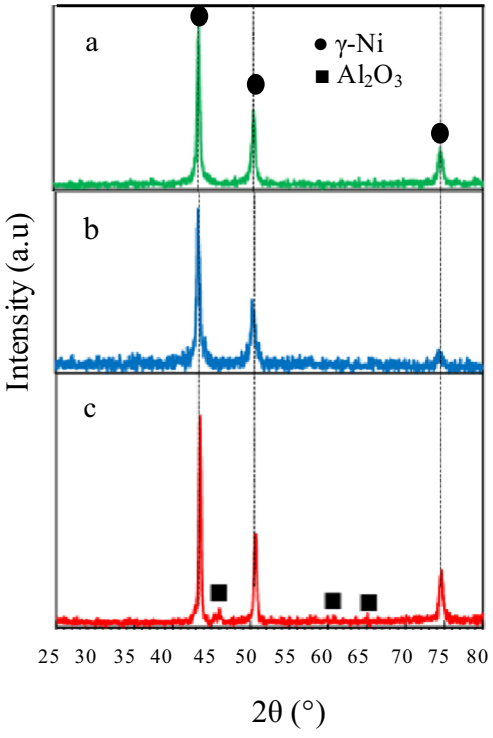

Fig. 7. XRD patterns of polished DED specimens and the feedstock powder (bottom), a) specimen extracted from built samples with the low energy input (settings 1 of Table 1), b) specimen extracted from built samples with the high energy input (settings 2 of Table 1) and c) powder.

3.3. Characterization after oxidation and corrosion exposures

The weight change of the as-built DED specimens exposed to ambient air for 168 h at 700, 800, and 900 °C is shown in Fig. 8. It can be seen that the samples produced with the low energy input had a lower weight increase at all three temperatures. The lower weight increase resulted from less oxygen uptake during the exposure, leading to the formation of fewer oxides.

The weight change of the samples exposed to ambient air with the Na_2SO_4 salt (corresponding to hot corrosion conditions) for 168 h at the temperatures of 700 and 900 °C is shown in Fig. 9. At 700 °C, the samples built with the high energy input showed a slightly lower weight decrease than the samples produced with the low energy input, whereas the results were reversed at 900 °C.

The XRD results of the as-built specimens exposed at three different temperatures of 700, 800 and 900 °C for 168 h are shown in Fig. 10. The phases found in the oxide layer on each specimen were almost identical. The identified peaks corresponded to oxides of various alloying elements contained in Alloy 718 (especially Cr, Ti, Fe, Nb, and Ni). The variation in the intensity of the peaks indicates the different extent of oxidation depending on the type of the oxide. The XRD peaks attributed to the γ-Ni(Cr) matrix phase in samples produced with the low energy input and exposed at 700 and 800 °C can be easier distinguished from the rest of the spectrum in comparison to the samples built with the high energy input. What is more, at all temperature levels, the intensity of the rest of the spectrum is lower for the samples built with the low energy input. This confirms that the oxide scale formed on the samples produced with the low energy input had probably a smaller thickness. This observation is in agreement with the lower weight change, thus thinner oxide layers, exhibited in Fig. 8.

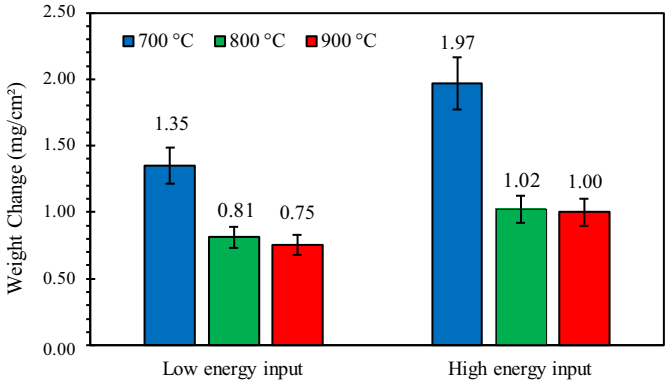

Fig. 8. Weight change of the as-built DED specimens after the oxidation tests exposed for 168 h.

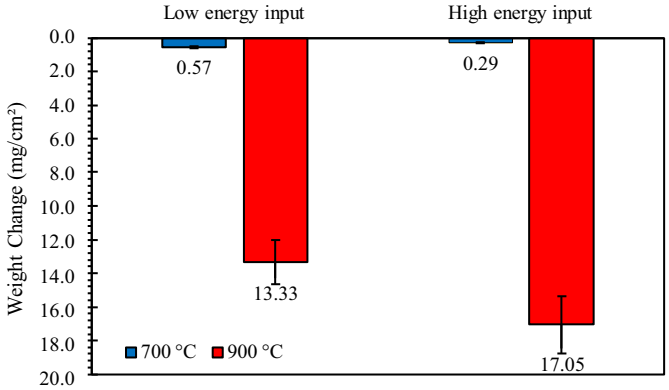

Fig. 9. Weight change of the as-built DED specimens after the hot corrosion tests exposed for 168 h.

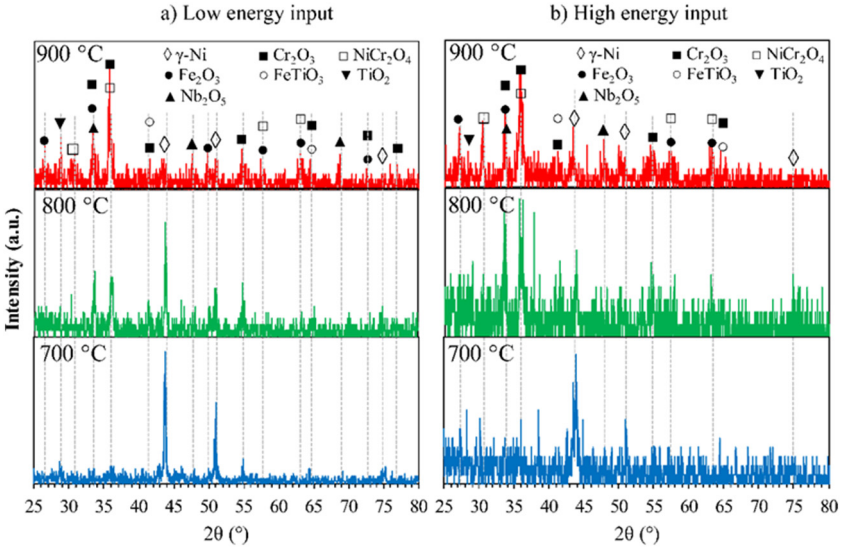

Fig. 10. XRD patterns of the oxidized DED specimens after the oxidation tests exposed for 168 h.

Fig. 11 shows the XRD patterns of the corroded DED specimens after 168 h of exposure in ambient air under the Na_2SO_4 salt at 700 and 900 °C. At the lower temperature only chromia scale along with γ-Ni was identified, while the phases found in the corrosion product formed on all the specimens at 900 °C were oxides of different alloying elements identical to the ones identified on oxidized specimens. The Fe_2O_3, Cr_2O_3, Nb_2O_5, $NiCr_2O_4$, TiO_2 and $FeTiO_3$ phases were characterized on all the analyzed specimens. Comparing the two batches of the specimens (built with the low and high energy inputs), it can be seen that the γ-Ni peaks were easier to be identified for the specimens exposed at 700 °C compared to the specimens exposed at 900 °C. Moreover, the overall higher intensity of the peaks related to other phases than γ-Ni, which characterize the specimens exposed at 900 °C, indicates the formation of a thicker layer of the corrosion products in this temperature compared to 700 °C.

Fig. 12 and Fig. 13 show the SEM cross-sectional images of the oxidized specimens after 168 h of exposure at 700, 800, and 900 °C as well as the corroded specimens under the Na_2SO_4 salt at 700 and 900 °C. As the temperature increased, the thickness of the formed oxides increased in all the specimens. At 700 and 800 °C, a continuous and very thin oxide scale formed on the surface, in agreement with the XRD results. Fig. 12 shows that the oxide formed at 900 °C on the specimens produced with the low energy input was thinner than the oxide formed on the other specimens. The oxide scales that formed on all the specimens at 900 °C consisted of a continuous external chromia scale enriched in Ti, Fe, Nb, and Ni as well as an internal oxide that was branched structure of alumina. The formation of the inner and also internal oxides (see Fig. 12 f) in the specimens produced with the high energy input was seen on the entire surface of the exposed specimens, whereas the oxide scale formed on the specimens built with the low energy input was rather external. Formation of inner and internal oxides is highly detrimental as oxygen diffuses through the base alloy via grain boundaries and adversely affects the corrosion performance. It is pertinent to mention here that the Laves (rich in Mo and Nb) and δ phases were detected in all the exposed specimens. Such phases can also be seen in the corroded specimens at 700 and 900 °C in Fig. 13. The formation of the Laves phases, showing as large white spots, can be easily identified in the corroded specimens. Specimens produced with the high energy input were characterized by a uniform distribution of the Lava phases. In addition, in these specimens, several internal defects in the form of pores and cracks were observed. The effect of these flaws formed during the DED process, as well as any AM or welding process, should not be ignored as it can accelerate the diffusion of corrosive species such as oxygen into the base alloy [19].

4. Discussion

Using the monitoring system based on the optical spectroscopy, we found the presence of Cr I spectral emission from the plasma plume above the melt pool, which is a clear indication of Cr vaporization, either directly from the melt pool of the already deposited material or the overheated powder particles flying through the laser beam. The phenomenon was limited to a few low-intensity lines in case of depositions performed using the low energy input, while it became very apparent during DED experiments with the high energy input, characterized by multiple intense Cr I spectral lines. These findings are consistent with the literature [4]. Further EDS analysis performed on the as-built specimens of material extracted from the built samples gave the evidence of lower Cr content in the samples where intense Cr I lines were detected during their deposition. Thus, these results support the claim of higher rate of Cr depletion from the alloy during the deposition with the high energy input. Despite the fact that the average percentage of Cr content of the samples manufactured with both the low and the high energy

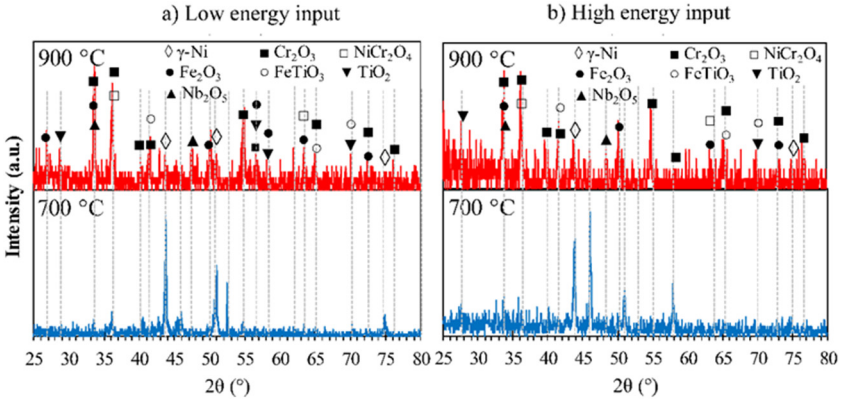

Fig. 11. XRD patterns of the corroded DED specimens after the hot corrosion tests exposed for 168 h.

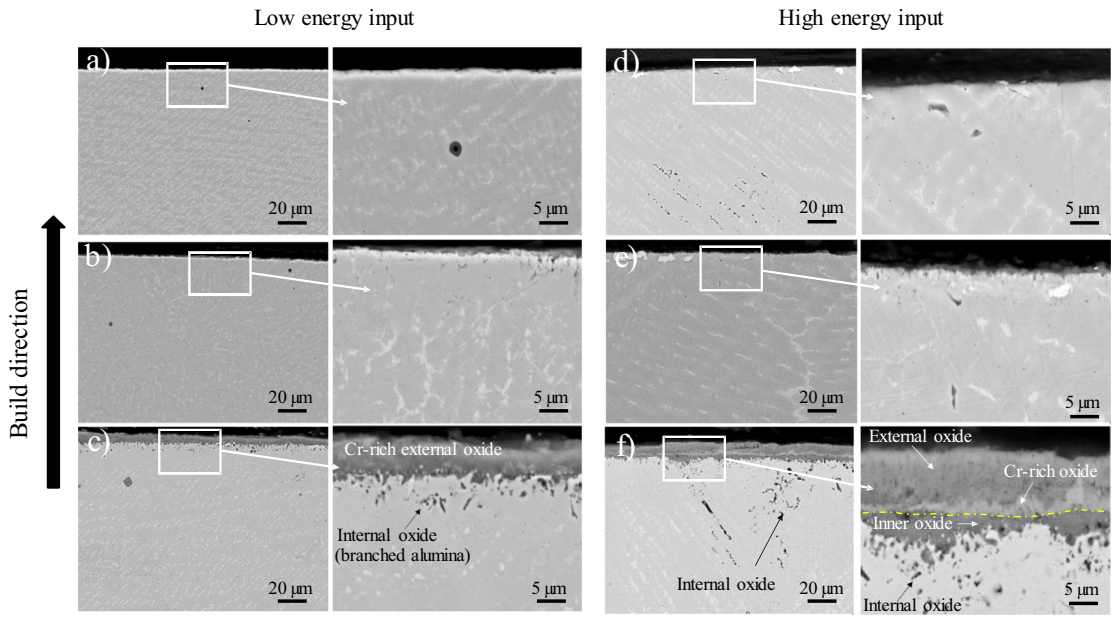

Fig. 12. SEM images (SE mode) of the cross-sections taken from the top layers of the oxidized DED samples after 168 h of exposure, specimens produced with the low energy input exposed at (a) 700 °C, (b) at 800 °C, and (c) at 900 °C, respectively, and specimens produced with the high energy input exposed at (d) 700 °C, (e) 800 °C, and (f) 900 °C.

input was still within the compositional specifications of the Alloy 718, the spectroscopic data gave an evident indication of Cr vaporization in the latter case, which demonstrates the high sensitivity of the monitoring technique. Indeed, the spectroscopic system was able to detect Cr compositional changes as small as 0.54 wt% due to variations in the applied laser power.

Although the variation of the chemical composition was relatively small, the materials deposited with the different energy inputs performed noticeably different during the material characterization tests. The specimens extracted from the samples built using the low energy input settings experienced lower weight change after the exposure to oxidation and hot corrosion environments at temperatures above 700 °C. For the same samples, the XRD results verified that the oxide scales and corrosion products formed were thinner than those of the specimens extracted from samples built with the high energy input. This was indicated by more clearly recognizable peaks characterizing γ-Ni phase, representing radiation reflected from the base matrix of Alloy 718. In addition to this, the intensity of the rest of the spectra was also lower for these specimens, thus indicating the lower extent of formed oxides and corrosion products. It is worth noticing that all of the samples performed better after being exposed to conditions of hot corrosion Type II than Type I, as in the later conditions, corrosion products contained not only the protective chromia scale but also diffused oxides of other alloying elements. The SEM analysis on the cross-sections of the exposed specimens showed less uniform layer of corrosion products for the samples built with the high energy input after oxidation and hot corrosion exposures at 900 °C as well as the presence of inner and internal oxides diffused through the matrix of the alloy, which indicates higher rate of material degradation. Moreover, the samples contained more Laves phase, which can be interpreted as nucleation sites for the formation and growth of the surface oxides.

A strong relationship was demonstrated between the spectroscopic data acquired in-line during the process and the properties of the deposited material in terms of chemical composition and high-temperature corrosion performance.

5. Conclusions

A miniature and fast spectrometer was used to acquire in-process optical emission radiated by the laser-matter interaction volume during DED of Alloy 718. The response of the detector was evaluated under

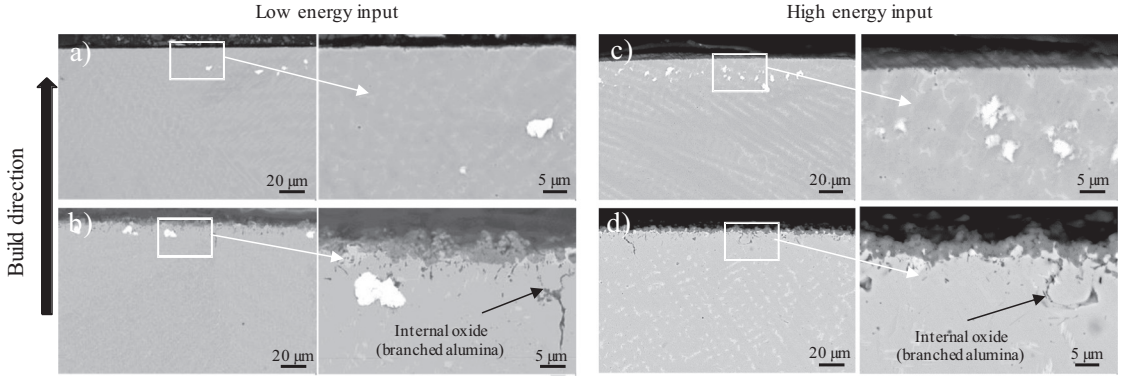

Fig. 13. SEM images (SE mode) of the cross-sections taken from the top layers of the corroded DED specimens under the Na_2SO_4 salt after 168 h of exposure, specimens produced with the low energy input at (a) 700 °C, (b) at 900 °C and specimens produced with the high energy input at (c) 700 °C, and (d) at 900 °C.

different process settings. In particular, two process conditions characterized by the high and low energy input onto the material were investigated. The spectroscopic data revealed conditions where Cr atoms were vaporized and depleted from the deposited Alloy 718 due to the high energy input. This was indicated by the presence of multiple, distinct and well recognizable spectral lines belonging to Cr I. Post-process EDS compositional analyses confirmed that the spectroscopic monitoring system has a high sensitivity, since differences of less than 1 wt% of Cr content were detected between specimens extracted from samples deposited with the different process settings. Therefore, this monitoring technology is proven to have the potential for detecting process conditions in which critical alloying elements vaporize from deposited alloys and thereby changing their compositions and material properties.

The Alloy 718 samples with the lower Cr content were overall characterized by impaired performance in most of the oxidation and high-temperature corrosion tests. The differences in the performance were not only attributed to the lower Cr content of the material but also to the different microstructure of the samples and the presence of defects which were dependent on the applied process conditions. The in-process plasma spectroscopy revealed this change of the process conditions owing to different levels of laser energy input and leading to different material properties. Thus, it has been demonstrated that plasma spectroscopy can be used as a base for a highly sensitive in-process monitoring system that can aid to sustain a good quality of produced AM part.

Data availability

The authors declare that the main data describing procedures, supporting the findings and conclusions of this study are available within the article. Extra data are available from the corresponding author upon request.

Funding

This work was supported by the Swedish Knowledge Foundation, Sweden - KK-stiftelsen within the project SUMANnext [grant number 20160281] and Sweden's innovation agency Vinnova within the project DigiAM [grant number 2016–04486].

CRediT authorship contribution statement

Agnieszka Kisielewicz: Investigation, Formal analysis, Writing - review & editing, Writing - original draft. **Esmaeil Sadeghi:** Investigation, Formal analysis, Writing - review & editing. **Fredrik Sikström:** Funding acquisition, Conceptualization, Investigation, Writing - review & editing. **Anna-Karin Christiansson:** Writing - review & editing, Supervision. **Gianfranco Palumbo:** Methodology, Writing - review & editing. **Antonio Ancona:** Conceptualization, Investigation, Writing - review & editing, Supervision.

Acknowledgements

The authors would like to thank Mr. Kjell Hurting at University West in Trollhättan, Sweden for his help with running the experiments as well as Mr. Omkar Aranke and Mrs. Paria Karimi at University West in Trollhättan, Sweden for their valuable help and advice in characterizing the samples and corrosion exposures.

References

[1] R.C. Reed, The Superalloys: Fundamentals and Applications, Cambridge University Press, 2008.
[2] B. Geddes, H. Leon, X. Huang, Superalloys: Alloying and Performance, ASM International, 2010.
[3] R. Liu, Z. Wang, T. Sparks, F. Liou, J. Newkirk, 13 - aerospace applications of laser additive manufacturing, in: M. Brandt (Ed.), Laser Addit. Manuf. Woodhead Publishing 2017, pp. 351–371, https://doi.org/10.1016/B978-0-08-100433-3.00013-0.
[4] T. DebRoy, H.L. Wei, J.S. Zuback, T. Mukherjee, J.W. Elmer, J.O. Milewski, A.M. Beese, A. Wilson-Heid, A. De, W. Zhang, Additive manufacturing of metallic components – process, structure and properties, Prog. Mater. Sci. 92 (2018) 112–224, https://doi.org/10.1016/j.pmatsci.2017.10.001.
[5] P.A.A. Khan, T. DebRoy, Alloying element vaporization and weld pool temperature during laser welding of AlSl 202 stainless steel, Metall. Trans. B. 15 (1984) 641–644, https://doi.org/10.1007/BF02657284.
[6] S.M. Thompson, L. Bian, N. Shamsaei, A. Yadollahi, An overview of Direct Laser Deposition for additive manufacturing; Part I: transport phenomena, modeling and diagnostics, Addit. Manuf. 8 (2015) 36–62, https://doi.org/10.1016/j.addma.2015.07.001.
[7] T. Mukherjee, J.S. Zuback, A. De, T. DebRoy, Printability of alloys for additive manufacturing, Sci. Rep. 6 (2016) https://doi.org/10.1038/srep19717.
[8] G.Y. Lai, High-Temperature Corrosion and Materials Applications, ASM International, 2007.
[9] B.J. Aalderink, R.G.K.M. Aarts, J.B. Jonker, J. Meijer, Weld plume emissions during Nd: YAG laser welding, Proc. Third Int. WLT-Conf. Lasers Manuf. 14-17 June 2005 Munich Ger 2005, p. 413.
[10] K. Bartkowiak, Direct laser deposition process within spectrographic analysis in situ, Phys. Procedia. 5 (2010) 623–629, https://doi.org/10.1016/j.phpro.2010.08.090.
[11] L. Song, J. Mazumder, Real time Cr measurement using optical emission spectroscopy during direct metal deposition process, IEEE Sens. J. 12 (2012) 958–964, https://doi.org/10.1109/JSEN.2011.2162316.
[12] D. De Baere, W. Devesse, B. De Pauw, L. Smeesters, H. Thienpont, P. Guillaume, Spectroscopic monitoring and melt pool temperature estimation during the laser metal deposition process, J. Laser Appl. 28 (2016), 022303. https://doi.org/10.2351/1.4943995.
[13] W. Ya, A.R. Konuk, R. Aarts, B. Pathiraj, B. Huis in 't Veld, Spectroscopic monitoring of metallic bonding in laser metal deposition, J. Mater. Process. Technol. 220 (2015) 276–284, https://doi.org/10.1016/j.jmatprotec.2015.01.026.
[14] C.B. Stutzman, A.R. Nassar, E.W. Reutzel, Multi-sensor investigations of optical emissions and their relations to directed energy deposition processes and quality, Addit. Manuf. 21 (2018) 333–339, https://doi.org/10.1016/j.addma.2018.03.017.
[15] S. Liu, W. Liu, M. Harooni, J. Ma, R. Kovacevic, Real-time monitoring of laser hot-wire cladding of Inconel 625, Opt. Laser. Technol. 62 (2014) 124–134, https://doi.org/10.1016/j.optlastec.2014.03.007.
[16] A. Kramida, Yu Ralchenko, J. Reader, NIST ASD Team, NIST Atomic Spectra Database, ver. 5.5.1 2017. https://physics.nist.gov/asd, Accessed date: 1 December 2017.
[17] A. Segerstark, J. Andersson, L.-E. Svensson, Investigation of laser metal deposited Alloy 718 onto an EN 1.4401 stainless steel substrate, Opt. Laser. Technol. 97 (2017) 144–153, https://doi.org/10.1016/j.optlastec.2017.05.038.
[18] E. Sadeghi, P. Karimi, S. Momeni, M. Seifi, A. Eklund, J. Andersson, Influence of thermal post treatments on microstructure and oxidation behavior of EB-PBF manufactured Alloy 718, Mater. Char. 150 (2019) 236–251.
[19] E. Sadeghi, P. Karimi, P. Zhang, R. Peng, J. Andersson, L. Pejryd, S. Joshi, Isothermal oxidation behavior of EBM-additive manufactured alloy 718, Proc. 9th Int. Symp. Superalloy 718 Deriv. Energy Aerosp. Ind. Appl. Springer International Publishing 2018, pp. 219–240.